

1 **A revisit of parametrization of downward longwave radiation in**
2 **summer over the Tibetan Plateau based on high temporal resolution**
3 **measurements**

4 Mengqi Liu^{a,c}, Xiangdong Zheng^d, Jinqiang Zhang^{a,b,c} and Xiangao Xia^{a,b,c}

5 ^a LAGEO, Institute of Atmospheric Physics, Chinese Academy of Sciences, Beijing,
6 100029, China

7 ^b Collaborative Innovation Center on Forecast and Evaluation of Meteorological
8 Disasters, Nanjing University of Information Science & Technology, Nanjing 210044,
9 China

10 ^c College of Earth and Planetary Sciences, University of Chinese Academy of Sciences,
11 Beijing, 100049, China

12 ^d Chinese Academy of Meteorological Sciences, Chinese Meteorological Bureau,
13 Beijing, 100081, China

14

15

Abstract

The Tibetan Plateau (TP) is one of research hot spots in the climate change research due to its unique geographical location and high altitude. Downward longwave radiation (DLR), as a key component in the surface energy budget, is of practical implications for radiation budget and climate change. A couple of attempts have been made to parametrize DLR over the TP based on hourly or daily measurements and crude clear sky discrimination methods. This study uses 1-minute shortwave and longwave radiation measurements at three stations over TP to parameterize DLR during summer months. Three independent methods are used to discriminate clear sky from clouds based on 1-minute radiation and Lidar measurements. This guarantees strict selection of clear sky samples that is fundamental for the parameterization of clear-sky DLR. Eleven clear-sky and four cloudy DLR parameterizations are examined and locally calibrated. Comparing to previous studies, DLR parameterizations here are shown be characterized by smaller root mean square error (RMSE) and higher coefficient of determination (R^2). Clear-sky DLR can be estimated from the best parametrization with RMSE of $3.8 \text{ W}\cdot\text{m}^{-2}$ and $R^2 > 0.98$. Systematic overestimation of clear-sky DLR by the locally calibrated parametrization in previous study is found to be approximately $25 \text{ W}\cdot\text{m}^{-2}$ (10%), which is very likely due to potential residual cloud contamination on previous clear-sky DLR parametrization. Cloud-base height under overcast conditions is shown to play an important role in cloudy DLR parameterization, which is considered in the locally calibrated parameterization over the TP for the first time. Further studies on DLR parameterization during nighttime and in seasons except summer are required for our better understanding of DLR's role in climate change based on 1-minute high-quality DLR measurements.

42 **1 Introduction**

43 The downward longwave radiation (DLR) at the Earth's surface is the largest
44 component of the surface energy budget, being nearly double the downward shortwave
45 radiation (DSR) (Kiehl and Trenberth, 1997). DLR has shown a remarkable increase
46 during the process of global warming (Stephens et al., 2012). This is closely related to
47 the fact that both a warming and moistening of the atmosphere (especially at the lower
48 atmosphere associated with the water vapor feedback) positively contribute to this
49 change. Understanding of complex spatiotemporal variation of DLR and its implication
50 is necessary for improving weather prediction, climate simulation as well as water
51 cycling modeling. Unfortunately, errors in DLR are considered substantially larger than
52 errors in any of the other components of surface energy balance, which is most likely
53 related to the lack of DLR measurements with high quality (Stephens et al., 2012).

54 The 2-sigma uncertainty of DLR measurement by using a well-calibrated and
55 maintained pyrgeometer is estimated to be 2.5% or $4 \text{ W} \cdot \text{m}^{-2}$ (Stoffel, 2005). However,
56 global-wide surface observations are very limited, especially in those remote regions.
57 On the other hand, it has been known for almost one century that clear-sky DLR is
58 determined by the bulk emissivity and effective temperature of the overlying
59 atmosphere (Ångström, 1918). Since these two quantities are not easily observed for a
60 vertical column of the atmosphere, clear-sky DLR is widely parameterized as a function
61 of surface air temperature and water vapor density, assuming that the clear sky radiates
62 toward the surface like a grey body at screen-level temperature. Dozens of
63 parameterization formulas of DLR have been developed in which clear-sky effective
64 emissivity (ϵ_c) is a function of the screen-level temperature (T) and water vapor pressure
65 (e), or simply in the localized coefficients with given functions. Two formulas, i.e., an
66 exponential function (Idso, 1981) and a power law function (Brunt, 1932; Swinbank,
67 1963), have been widely used to depict the relationship of ϵ_c to T and e . The coefficients
68 of these functions are derived by a regression analysis of collocated measurements of
69 T , e and DLR. Most of these proposed parameterizations are empirical in nature and
70 only specific for definite atmospheric condition. An exception is that Brutsaert (1975)
71 developed a model based on the analytic solution of the Schwarzschild's equation for a

72 standard atmospheric lapse rates of T and e . Prata (1996) found that the precipitable
73 water content (w) was much better to represent the effective emissivity of the
74 atmosphere than e , which was loosely based on radiative transfer simulations. Dilley
75 and O'Brien (1998) adopted this scheme but tuned empirically their parameterization
76 using an accurate radiative transfer model. Since DLR is to some extent impacted by
77 water vapor and temperature profile (especially in case of existence of an inversion
78 layer) and diurnal variation of T , a new model with two more coefficients considering
79 these effects was developed (Dupont et al., 2008a).

80 In the presence of clouds, total effective emissivity of the sky is remarkably
81 modulated by clouds. The existing clear-sky parameterization should be modified
82 according to the cloud fraction (CF) and other cloud parameters such as cloud base
83 height (CBH). CF is generally used to represent a fairly simple cloud modification
84 under cloudy conditions. Dozens of equations with cloudiness correction have been
85 developed and evaluated by DLR measurements across the world (Crawford and
86 Duchon, 1999; Niemela et al., 2001). CF can be obtained by trained human observers
87 (Iziomon et al., 2003) or derived from DSR (Crawford and Duchon, 1999) and DLR
88 measurements (Durr and Philipona, 2004). High temporal resolution of DSR or DLR
89 measurements (for example, 1-minute) can also provide cloud type information
90 (Duchon and O'Malley, 1999), and thereby allow to consider potential effects of cloud
91 types on DLR (Orsini et al., 2002).

92 With an average altitude exceeding 4 km above the sea level (ASL), the Tibetan
93 Plateau (TP) exerts a huge influence on regional and global climate through mechanical
94 and thermal forcing because of its highest and most extensive highland in the world
95 (Duan and Wu, 2006). TP, compared to other high altitude regions and the poles, has
96 been relatively more sensitive to climate change. The most rapid warming rate over the
97 TP occurred in the latter half of the 20th century was likely associated with relatively
98 large increase in DLR. Duan and Wu (2006) indicated that increase in low level
99 nocturnal cloud amount and thereby DLR could partly explain the increase in the
100 minimum temperature, despite decrease in total cloud amount during the same period.
101 By using observed sensitivity of DLR to change in specific humidity for the Alps,

102 Rangwala et al. (2009) suggested that increase in water vapor appeared to be partly
103 responsible for the large warming over the TP. Since the coefficients of certain
104 empirical parameterizations and their performances showed spatiotemporal variations,
105 establishment of localized DLR parameterizations over the TP is of highly significance.
106 Further studies on DLR, including its spatiotemporal variability, its parameterization as
107 well as its sensitivity to changes in atmospheric variables, would be expected to
108 improve our understanding of climate change over the TP (Wang and Dickinson, 2013).

109 DLR measurements from high quality radiometer with high temporal resolution
110 over the TP are quite scarce. To the best of our knowledge, there are very few
111 publications on DLR and its parameterization over the TP. Wang and Liang (2009)
112 evaluated clear-sky DLR parameterizations of Brunt (1932) and Brutsaert (1975) at 36
113 globally distributed sites, in which DLR data at two TP stations were used. Yang et al.
114 (2012) used hourly DLR data at 6 stations to study major characteristics of DLR and to
115 assess the all-sky parameterization of Crawford and Duchon (1999). Zhu et al. (2017)
116 evaluated 13 clear-sky and 10 all-sky DLR models based on hourly DLR measurements
117 at 5 automatic meteorological stations. The Kipp & Zonen CNR1 is composed of CM3
118 pyranometer and CG3 pyrgeometer that are used to measure DLR and DSR,
119 respectively. The CG3 is the second class radiometer according to the International
120 Organization for Standardization (ISO) classification. The root mean square of hourly
121 DLR is less than 5 Wm^{-2} after field recalibration and window heating correction
122 (Michel et al., 2008). Note that human observations of cloud every 3-6 hours or hourly
123 DLR and DSR data are respectively used to determine clear sky and cloud cover in
124 these previous studies.

125 In order to further our understanding of DLR and DSR over the TP, measurements
126 of 1-minute DSR and DLR at 3 stations over the TP using state-of-the-art instruments
127 have been performed in summer months since 2011. These data provide us opportunity
128 to evaluate clear-sky DLR models and quantitatively assess cloud impacts on DLR.
129 This study makes progress in the following aspects as compared to previous studies: 1)
130 clear-sky discrimination and CF estimation are based on 1-minute DSR and DLR
131 measurements that are objective in nature; 2) misclassification of cloudiness into cloud-

132 free skies would be minimized by adopting strict cloud-screening procedures based on
133 1-minute DSR, DLR and Lidar measurements; 3) potential effects of CBH on DLR are
134 also investigated. Localized parameterizations of clear-sky and all-sky DLRs are finally
135 achieved, which would be expected to improve DLR estimations over the TP.

136

137 **2. Site, Instrument and Data**

138 Measurements of DLR and DSR conducted 1~4 months over the TP at three
139 stations (Table 1), including Nagqu (NQ, 92.04°E, 31.29°N, 4507 m ASL), Nyingchi
140 (NC, 94.2°E, 29.4°N, 2290 m ASL) and Ali (AL, 80°E, 32.5°N, 4287 m ASL) are used
141 for the DLR parameterization. DLR and DSR were respectively measured by CG4 and
142 CM21 radiometers (Kipp & Zonen, Delft, Netherlands). The sampling frequency is 1
143 Hz and the averages of the samples over 1-minute intervals are logged on a Campbell
144 Scientific CR23X datalogger. Simultaneous 1-minute averages of T and e are taken
145 from the automatic meteorological stations. With the aid of its specific material and
146 unique construction, CG4 is designed for the DLR measurement with high reliability
147 and accuracy. Window heating due to absorption of solar radiation in the window
148 material, the major error source of DLR measurement, is strongly suppressed by its
149 unique construction conducting away the absorbed heat very effectively. CM21 is a
150 high performance research grade pyranometer. Introduction of individually optimized
151 temperature compensation for CM21 makes it having much a smaller thermal offset
152 than CM3. The installation of the CG4 and CM21 on the Kipp & Zonen CV2 ventilation
153 unit prevents dew deposition on the window of the CG4 and the quartz dome of the
154 CM21. The radiometers are calibrated before and after field measurements to the
155 standards held by the China National Centre for Meteorological Metrology.

156 A Micropulse Lidar (MPL-4B, Sigma Space Corporation, United States) was
157 installed site-by-site with radiometers. The Nd:YLF laser of the MPL produces an
158 output power of 12 μ J at 532 nm. The repetition rate is 2500 Hz. The vertical resolution
159 of the MPL data is 30 m and the integration time of the measurements is 30s. The MPL
160 backscattering profiles are used to identify the cloud boundaries and derive the CBHs
161 (He et al., 2013). The dataset contains about 700 hours of coincident DLR, DSR, Lidar

162 and meteorological measurements.

163 DLR and DSR were also measured at Lhasa (91.1°E, 29.9°N, 3649 m ASL) during
164 summer in 2012 using the same instruments as those in other stations. Lhasa data are
165 mainly used for independent validation because of no Lidar data there.

166

167 **3. Methods**

168 **3.1 Clear-sky discrimination**

169 Clear skies should be discriminated from cloudy conditions before performing
170 DLR parametrization, which is achieved by the synthetical analysis of DSR, DLR, and
171 CBH from MPL.

172 Following the method initiated by Crawford and Duchon (1999), we calculate two
173 quantities reflecting DSR magnitude and variability based on 1-minute observed DSR
174 (DSR_{obs}) and calculated clear-sky DSR (DSR_{cal}) values. DSR_{cal} is calculated by the
175 model C of Iqbal (1983), in which direct and diffuse DSR are parametrized separately.
176 Direct DSR (DSR_{dir}) is calculated as follows.

$$177 \quad DSR_{dir} = S_0 \tau_r \tau_w \tau_o \tau_a \tau_g \quad (1)$$

178 where τ_r , τ_w , τ_o , τ_a and τ_g are transmittances due to Rayleigh scattering, water
179 vapor absorption, ozone absorption, aerosol extinction and absorption by uniformly
180 mixed gases O₂ and CO₂, respectively. Diffuse radiation is estimated as the sum of
181 Rayleigh and aerosol scattering as well as multiple reflectance. Total ozone column
182 (DU) is provided by Brewer spectrophotometer. w values (cm) are from Vaisala-92
183 radiosonde profiles in AL and Global Position System measurements in NC and NQ,
184 respectively. They are used to create linear regression relationship to collocated ground
185 level e (hPa) measurements, which is then used to estimate w from 1-minute
186 measurements of e . Ångström wavelength exponent and Ångström turbidity are from
187 CIE-318 sunphotometer observations in NC and AL, while in NQ we adopt the same
188 value as that in AL. Mean single scattering albedo retrieved from CIE-318 observation
189 in Lhasa (91.13, 29.67, 3663m) is 0.90 (Che et al., 2019), which is used in three stations.
190 Surface Albedo is 0.25 and 0.22 in AL and NQ according to in situ measurements (Liang
191 et al., 2012). In NC, it is 0.183 (Zhao et al., 2011).

192 DSR_{cal} values are first scaled to a constant value of $1400 \text{ W}\cdot\text{m}^{-2}$ for each minute of
193 each day. We adopt this value according to Duchon and O'Malley (1998) and Long and
194 Ackerman (2000), which only favors for a clear presentation of the normalized and
195 observed DSR values in the same figure. Afterwards, DSR_{obs} values are scaled by
196 multiplying the same set of scale factors. Finally, the mean and standard deviation of
197 the scaled DSR in a 21-minute moving window (± 10 minute centered on the time of
198 interest) are used for cloud screening. Selection of the width of 21-minute is empirical
199 but a consequence of having a reasonable time span for estimating the mean and
200 variance (Duchon and O'Malley, 1999). Clear-sky DSR should satisfy three
201 requirements: 1) ratio of DSR_{obs} to DSR_{cal} is within 0.95 to 1.05; 2) difference between
202 scaled DSR_{obs} and DSR_{cal} is less than $20 \text{ W}\cdot\text{m}^{-2}$; and 3) standard deviation (δ) of scaled
203 DSR_{obs} in a 21-minute moving window is less than $20 \text{ W}\cdot\text{m}^{-2}$.

204 Temporal variability of DLR is also used for cloud screening according to Marty
205 and Philipona (2000) and Sutter et al. (2004). Here, δ of scaled DLR (scaled to 500
206 $\text{W}\cdot\text{m}^{-2}$) in a 21-minute moving window is used for this purpose. Cloud-free sample is
207 determined if δ is less than $5 \text{ W}\cdot\text{m}^{-2}$.

208 Since both DSR and DLR experience difficulties in detecting clouds in the portion
209 of the sky far away from the sun (Duchon and O'Malley, 1999) or high-altitude cirrus
210 clouds (Dupont et al., 2008b), coincident MPL backscatter measurements are used to
211 strictly select clear-sky samples. There should be a cloud element somewhere in the sky
212 when MPL identifies cloud, it is thus required that no clouds are detected by MPL in a
213 21-minute moving window, otherwise it is defined as cloudy.

214 Given the fact that these methods are complementary to each other to some extent
215 (Orsini et al., 2002), we use the following strategy to guarantee a proper selection of
216 clear-sky samples. If DSR, DLR and MPL measurements at the time of interest
217 synchronously satisfy these specified clear-sky conditions, the sample is thought to be
218 taken under unambiguously cloud-free condition; on the contrary, the measurement are
219 made under unambiguously cloudy condition if any method suggests cloudy. Our
220 following clear-sky and cloudy DLR parameterizations are respectively based on
221 measurements under unambiguously cloud-free (8195 minutes) and cloudy conditions

222 (69318 minutes).

223 Fig. 1 shows an example of clear sky discrimination results based on our method.
224 DSR_{obs} presents a smooth temporal variation from sunrise to about 14:00 (LST), being
225 consistent with DSR_{clr} . Similarly, DLR also varies very smoothly during the same
226 period when 21-minute standard deviations of DLR are $< 5 \text{ W} \cdot \text{m}^{-2}$. Both facts suggest
227 sunny and cloudless skies. This inference is supported by MPL that suggests no cloud
228 detected overhead. Contrarily, an abruptly changes of 1-minute DSR_{obs} and DLR are
229 evident during 14:00~17:00 LST and we can see DSR_{obs} occasionally exceeds the
230 expected DSR_{clr} , indicating frequent occurrence of fair weather cumuli clouds. MPL
231 detect a persistent thin cloud layer at 4 km above ground, which agrees with DSR and
232 DLR measurements very well.

233

234 3.2 Cloud fraction estimation

235 Given synoptic cloud observations are very limited and temporally sparse, various
236 parameterizations using DSR or DLR data have been developed to estimate CF (e.g.,
237 Deardorff, 1978; Marty and Philipona, 2000; Durr and Philipona, 2004; Long et al.,
238 2006; Long and Turner, 2008). Because of good agreement between clear-sky DSR_{obs}
239 and DSR_{cal} calculated by the Iqbal C calculations (Iqbal, 1983; Gubler et al., 2012),
240 with mean bias of $1.7 \text{ W} \cdot \text{m}^{-2}$ and root mean square error (RMSE) of $10.7 \text{ W} \cdot \text{m}^{-2}$ (not
241 shown), we use Deardorff (1978)'s method to calculate CF from DSR_{obs} and DSR_{cal} .
242 The method is based on a fairly simple cloud modification to DSR as follows.

$$243 \quad CF = 1 - \frac{DSR_{obs}}{DSR_{cal}} \quad (2)$$

244 CF (no unit) has values ranging from 0 to 1. To avoid the error caused by abrupt
245 DSR variation, 21-minute mean DSR value rather than its instantaneous measurements
246 are used here.

247

248 4 Results

249 4.1 Clear-sky DLR parameterization evaluation and localization

250 Eleven clear-sky DLR (DLR_{clr}) parameterizations (Table 2) are evaluated based

251 on 1-minute DLR measurements under unambiguously cloud-free conditions. To
252 compare the performance of these 11 models, RMSE and the coefficient of
253 determination (R^2) are shown by a Taylor diagram in Fig. 2(a). Relatively smaller
254 RMSE (generally $< 15 \text{ W}\cdot\text{m}^{-2}$) and larger R^2 (>0.95) are derived for the Brutsaert (1975);
255 Konzelmann (1994), Dilley and O'Brien (1998) and Prata (1996) models. This is likely
256 because these parameterizations were developed in cool and dry areas, for example, in
257 England (Brutsaert, 1975); in Greenland (Konzelmann, 1994) and dry desert region in
258 Australia (Prata, 1996). The climate in those areas is likely similar to that over the TP
259 to some extent, so those parameterizations are expected to perform well. The higher
260 RMSE ($>37 \text{ W}\cdot\text{m}^{-2}$) and the lower R^2 (~ 0.7) are derived for Swinbank (1963) and Idso
261 and Jackson (1969) models. This can be partly explained by the fact that only T is used
262 in these two methods. Previous studies suggests substantial uncertainty (RMSE >37.5
263 $\text{W}\cdot\text{m}^{-2}$ and $R^2 < 0.75$) if water vapor effect on DLR_{clr} is not accounted for (Duarte et al.,
264 2006). Since w is very low over the TP and thereby DLR is highly sensitive to variation
265 of w in that case, much more attention should be paid to water vapor effect on the
266 parameterization of DLR_{clr} .

267 The coefficients in eleven parameterizations (Table 2) were originally calibrated
268 and determined in different geographical locations; therefore, they may not be the
269 optimal values for the TP. Thus we take use of 1-minute clear-sky DLR samples to
270 locally calibrate the parameters of these parametrizations. We use 10-fold cross-
271 validation method to determine the parameters. This is a widely used method to
272 estimate the skill of a regression model on unseen data. It is expected to result in a less
273 biased or less optimistic estimate of the model skill than other methods, such as a simple
274 train/test split (James et al., 2013). All the data was randomly dividing into 10 groups
275 of approximately equal size, the coefficients are computed by using 9 groups as training
276 set, and the remaining 1 group is used as validation. This procedure is repeated 10 times
277 to get the representational value of coefficients (with the lowest test error).

278 The coefficient values derived from the non-linear least-squares fitting of the
279 DLR_{clr} parameterizations (Table 2) over the TP are presented in Table 3. For each fitted
280 parameterization, we calculated RMSE and R^2 and the results are shown in Fig. 2b.

281 When using the parameterizations with the locally fitted parameters, the accuracy of
 282 the parameterization relative to the published values is obviously improved. Most
 283 RMSEs are $< 10 \text{ W}\cdot\text{m}^{-2}$ except the parameterization proposed by Swinbank (1963) and
 284 Idso and Jackson (1969) that still produce the worst results (with R^2 of 0.71 and RMSE
 285 of $15 \text{ W}\cdot\text{m}^{-2}$) even after the parameters are locally calibrated.

286 The Dilley and O'Brien (1998)'s parameterization, which is initially developed by
 287 considering the adaptation of climatological diversities, is expected to be able to fit the
 288 measurements in tropical, mid-latitude and Polar Regions. This expectation is verified
 289 by its wide deployment in DLR_{clr} estimations in different climate regimes and altitude
 290 levels, for example, in the tropical lowland (eastern Pará state, Brazil) and the mild
 291 mountain area (Boulder, the United States) (Marthews et al., 2012; Li et al., 2017).
 292 The present study confirms that Dilley and O'Brien (1998) is the best clear-sky
 293 parameterization over the TP. The locally calibrated equation is as follows.

$$294 \quad \text{DLR}_{\text{clr}} = -2.53 + 158.10 \times \left(\frac{T}{273.16}\right)^6 + 106.40 \times \left(\frac{46.50 \times e}{2.50 T}\right)^{\frac{1}{2}} \quad (3)$$

295 Where T and e represent air temperature (K) and water vapor pressure (hPa),
 296 respectively (T and e have the same meaning and unit in following equations if not
 297 specified). The RMSE and R^2 of Eq.(3) are $\sim 3.8 \text{ W}\cdot\text{m}^{-2}$ and > 0.98 respectively, which
 298 are substantially lower than those in previous studies over the TP, for example, the
 299 RMSE was $9.5 \text{ W}\cdot\text{m}^{-2}$ (Zhu et al., 2017). The Dilley and O'Brien (1998)'s
 300 parameterization was suggested to be the most reliable estimates of DLR_{clr} over the TP
 301 (Zhu et al., 2017). Note that the parameters here differ quite a lot from their values (Zhu
 302 et al., 2017), as shown in Eq. (4).

$$303 \quad \text{DLR}_{\text{clr}} = 30.00 + 157.00 \times \left(\frac{T}{273.16}\right)^6 + 97.93 \times \left(\frac{46.50 \times e}{2.50 T}\right)^{\frac{1}{2}} \quad (4)$$

304 Fig.3 compares instantaneous clear-sky DLR data from measurements against
 305 calculations by Eq. (3) of this study and by Eq. (4) from Zhu et al. (2017). The former
 306 performs very well as shown by an overwhelmingly large number of data points falling
 307 along or overlapping the 1:1 line. By contrast, the latter overestimates DLR by $25 \text{ W}\cdot\text{m}^{-2}$
 308 (10%) . This difference is not very likely due to different DLR measurements used to
 309 produce Eq. (3) and (4) giving the following considerations. First, this systematic

310 overestimation is much larger than the expected uncertainty of DLR measurements (2.5%
311 or $4 \text{ W}\cdot\text{m}^{-2}$) (Stoffel, 2005). More important, comparison of cloudy DLR
312 parameterizations between this study and Zhu et al. (2017) showed good agreement
313 (not shown). Note that only 1-hour CG3 DLR observations are used for clear sky
314 discrimination in Zhu et al. (2017). This method was shown to be very likely
315 contaminated by the thin high cloud (Sutter et al., 2004). This certainly would produce
316 an overestimation of clear sky DLR parameterization since larger DLRs are associated
317 with potential residual clouds relative to real clear-sky DLRs.

318

319 **4.2 Parameterization of cloudy-sky DLR**

320 Parameterizations of cloudy-sky DLR (DLR_{cld}) are based on estimated DLR_{clr}
321 coupled with the effect of cloudiness or cloud emissivity, which depends primarily on
322 CF as well as other cloud parameters, like CBH and cloud type (Arking, 1990; Viúdez-
323 Mora et al., 2015). Four parameterizations (Table 4), which modifies the bulk
324 emissivity depending on CF, are assessed and locally calibrated in this section.

325 DLR_{clr} is estimated according to Eq. (3). The fitted values of the coefficients (using
326 10-Fold Cross-Validation) of the four cloudy parameterizations are presented in Table
327 4. RMSE and R^2 of original and locally fitted parameterizations over the TP are
328 presented in Fig. 4.

329 Relative to clear-sky conditions, cloudy parameterizations using the given
330 parameters have higher error RMSE (generally exceeding $35 \text{ W}\cdot\text{m}^{-2}$) except that
331 developed by Jacobs (1978) (RMSE of $18 \text{ W}\cdot\text{m}^{-2}$). R^2 was generally smaller than 0.9.
332 RMSE values decrease significantly in Maykut and Church (1973) and Sugita and
333 Brutsaert (1993) as locally calibrated parameters are used. Relative smaller and almost
334 no RMSE improvements are found for the methods developed by Konzelmann (1994)
335 and Jacobs (1978).

336 Eq. (5) shows the best cloudy-sky parameterization over the TP by combining the
337 clear-sky parameterization of Dilley and O'Brien (1998) with the cloud modulation
338 correction scheme of Jacobs (1978).

339
$$\text{DLR}_{\text{cld}} = (1 + 0.23 \times \text{CF}) \times \left(59.38 + 113.70 \times \left(\frac{T}{273.16} \right)^6 + 96.96 \times \left(\frac{46.50 \times \frac{\epsilon}{T}}{2.50} \right)^{\frac{1}{2}} \right) \quad (5)$$

340 RMSE and R^2 are $\sim 18 \text{ W} \cdot \text{m}^{-2}$ and ~ 0.89 respectively. RMSE here is close to $15 \text{ W} \cdot \text{m}^{-2}$
 341 obtained in different altitude areas in Swiss (Gubler et al., 2012) and slightly lower than
 342 $23 \text{ W} \cdot \text{m}^{-2}$ obtained in mountain area in Germany (Iziomon et al., 2003). Comparing to
 343 previous studies over the TP (RMSE of $22 \text{ W} \cdot \text{m}^{-2}$ in Zhu et al., 2017), our cloudy model
 344 produces better results.

345 In order to validate the newly developed DLR parameterizations, clear-sky and
 346 cloudy-sky DLR parameterizations are validated against DLR measurements at Lhasa.
 347 The results are shown in Fig. 5. Compared to the existed parameterizations, the Eq.(3)
 348 and Eq.(5) produce the smallest bias (both less than $2 \text{ W} \cdot \text{m}^{-2}$) and RMSE (Eq.(3)'s is
 349 less than $5 \text{ W} \cdot \text{m}^{-2}$ and Eq.(5)'s is less than $25 \text{ W} \cdot \text{m}^{-2}$). This independently demonstrates
 350 the improved DLR parameterizations can be used in other stations over the TP.

351

352 **4.3 Effect of CBH on DLR under Overcast Conditions**

353 Since clouds behave approximately as a blackbody, the most relevant cloud
 354 parameter (besides CF) to DLR under overcast skies (DLR_{ovc}) is CBH (Kato et al, 2011;
 355 Viúdez-Mora et al., 2015): firstly, CBH defines the temperature of the lowest cloud
 356 boundary, which through the Stefan-Boltzmann law drives the cloud emittance;
 357 secondly, DLR emitted by the atmospheric layers above a cloud is totally absorbed by
 358 the cloud itself (clouds are thick enough). Radiative transfer model simulation has
 359 suggested that CBH under overcast conditions is an important modulator for DLR. The
 360 cloud radiation effect (CRE), the difference between DLR_{obs} and DLR_{clr} , decreases with
 361 increasing CBH at a rate of $4\sim 12 \text{ W} \cdot \text{m}^{-2}$ that depends on climate profiles (Viúdez-Mora
 362 et al., 2015). This indicates that overcast DLR parameterization would be improved if
 363 CBH is considered.

364 A close relationship between CRE and CBH under overcast conditions over the TP
 365 is presented in Fig 6. Compared to Viúdez-Mora (2015) results derived at Girona, Spain,
 366 a mid-latitude site with low altitude, CRE over the TP is generally lower by $5\sim 10 \text{ W} \cdot \text{m}^{-2}$
 367 ². This is likely because clouds over the TP with the same CBH as that at Girona have

368 relatively lower temperature, thereby producing lower radiative effect on DLR. CRE
369 generally decreases as CBH increases. The result agrees with the expectation since
370 CBH influence on DLR should decrease as CBH increases as a result of increasing
371 water vapor effects on DLR. CRE is about $70 \text{ W}\cdot\text{m}^{-2}$ for clouds $< 1 \text{ km}$ and decreases
372 to $\sim 40 \text{ W}\cdot\text{m}^{-2}$ for clouds at 3~4 km in TP. The decreasing rate of CRE with CBH is
373 estimated to be $-9.8 \text{ W}\cdot\text{m}^{-2}\cdot\text{km}^{-1}$ over the TP that agrees with model simulations
374 (Viúdez-Mora et al., 2015).

375 Since CBH effect on overcast DLR is apparent, we introduced a modified
376 parameterization to consider CBH effect on DLR under overcast conditions as follows.
377 The calculated DLR_{ovc} ($\text{DLR}_{\text{ovc}}^{\text{cal}}$) is equal to DLR_{clr} times 1.23 due to CF of 1 in Eq. 5
378 that is irrelevant to CBH. On the other hand, the measured DLR_{ovc} ($\text{DLR}_{\text{ovc}}^{\text{obs}}$) is closely
379 related to CHB as shown in Fig. 6, so we calculated the ratio of $\text{DLR}_{\text{ovc}}^{\text{obs}}$ to the
380 corresponding $\text{DLR}_{\text{ovc}}^{\text{cal}}$ that showed a linear relationship to CBH, as shown in Fig.7. A
381 linearly fitted equation was then established between this ratio and CHB. DLR_{ovc} is
382 finally parameterized as follows.

$$383 \quad \text{DLR}_{\text{ovc}} = 1.23 \times \text{DLR}_{\text{clr}} \times (1.07 - 0.046 \times \text{CBH}) \quad (6)$$

384 Where CBH has unit of km. The bias and RMSE of Eq. (6) between measurements
385 and calculations are $-2.15 \text{ W}\cdot\text{m}^{-2}$ and $19.79 \text{ W}\cdot\text{m}^{-2}$, respectively, which are substantially
386 lower than that of Eq. (5) ($10.3 \text{ W}\cdot\text{m}^{-2}$ and $21.4 \text{ W}\cdot\text{m}^{-2}$) under overcast conditions. This
387 indicates a remarkable improvement in the estimation of DLR under overcast
388 conditions by introducing CBH to the DLR parameterization, therefore, introduce of
389 such instruments as ceilometer to measure CBH is highly significance for studying
390 cloud's impacts on DLR.

391

392 **5 Discussion and conclusions**

393 The parameterization of clear-sky DLR requires a well-defined distinction
394 between clear-sky and cloudy-sky situations that commonly depends on human cloud
395 observations 4~6 times each day. Human observation is subjective in nature and its low
396 temporal resolution cannot resolve dramatic high-resolution variation of clouds.

397 Furthermore, synoptic human cloud observations show the tendency to stronger weight
398 to the horizon that DLR is not highly sensitive (Marty and Philipona, 2004). Clear sky
399 discrimination based on hourly DSR or DLR measurements also tends to be very
400 suspect of residual clouds due to their low temporal resolution. Parameterization of
401 clear-sky DLR based on these two methods is hence very likely biased as a consequence
402 of selection of cloud contaminated clear-sky measurements. This would result in biased
403 estimation of cloud DLR effect since it is the difference between clear-sky and
404 measured all-sky DLRs (Dupont et al., 2008b).

405 Using 1-minute DSR and DLR at 3 stations over the TP, DLR parameterizations
406 are evaluated and localized parameterizations have been developed based on a
407 comprehensive cloud-screening method. We test the fitted parameterizations based on
408 independent DLR measurements at Lhasa. Potential CBH effect on overcast DLR is
409 experimentally determined. Major conclusions are as follows.

410 Among 11 clear-sky DLR parameterizations tested in this study, two methods
411 using only atmospheric temperature largely deviate from other parameterizations. The
412 best method suitable for TP is the parameterization developed by Dilley and O'Brien
413 (1998). DLR estimation can be improved by localization of these parameterizations.
414 Locally calibrated parameterization can produce clear sky DLR with RMSE of 3.8
415 $W \cdot m^{-2}$.

416 Overcast DLR is highly sensitive to CBH. The parameterization can be
417 substantially improved by consideration of CBH effect. The bias between empirically
418 parameterized calculations and measurements decreases from 10.3 to 1.3 $W \cdot m^{-2}$.

419 The focus of this study is on daytime DLR parameterization over the TP since DSR
420 is used in the cloud-screening method. Given a significant role of DLR played in the
421 surface energy budget during nighttime, it is highly desirable to perform further study
422 on the nighttime DLR parametrization. These results are based on summer DLR
423 measurements, so the conclusions here need to be further tested in other seasons,
424 especially in winter when an increasing tendency of DLR has been observed (Rangwala
425 et al., 2009). Further investigations on these issues are expected to shed new light on
426 how and why DLR has changed over the TP. Our results clearly showed substantial

427 CBH effect on overcast DLR, which would be considered in future when ceilometer is
428 widely used to measure CBH.

429

430 Acknowledgements: This work was supported by the Strategic Priority Research
431 Program of Chinese Academy of Sciences (XDA17010101), the National Key R&D
432 Program of China (2017YFA0603504), the National Natural Science Foundation of
433 China (91537213 and91637107), the Special Fund for Meteorological Research in the
434 Public Interest (GYHY201106023), and the Science and Technological Innovation
435 Team Project of Chinese Academy of Meteorological Science (2013Z005) respectively
436 support the observations at AL, NQ and NC. We greatly appreciate Dr. Q. He for
437 providing the MPL Lidar measurement images and derived CBH data.

438 **References**

- 439 Ångström, A.: A study of the radiation of the atmosphere, Smithsonian Miscellaneous
440 Collection, 65, 1–159, 1915.
- 441 Arking, A.: The radiative effects of clouds and their impact on climate, Bull. Am.
442 Meteorol. Soc., 72, 795-813, 10.1175/1520-
443 0477(1991)072<0795:Treoca>2.0.Co;2, 1991.
- 444 Brunt, D.: Notes on radiation in the atmosphere, Q. J. Roy. Meteorol. Soc., 58, 389–
445 420, 1932.
- 446 Brutsaert, W.: On a derivable formula for long-wave radiation from clear skies, Water
447 Resource Res., 11, 742–744, 1975.
- 448 Carmona, F., Rivas, R., and Caselles, V.: Estimation of daytime downward longwave
449 radiation under clear and cloudy skies conditions over a sub-humid region, Theor.
450 Appl. Climatol., 115, 281-295, 10.1007/s00704-013-0891-3, 2014.
- 451 Che, H. Z., Zhao, H. J., Wu, Y. F., Xia, X. G., Zhu, J., Wang, H., Wang, Y. Q., Sun, J.
452 Y., Yu, J., Zhang, X. Y., and Shi, G. Y.: Analyses of aerosol optical properties and
453 direct radiative forcing over urban and industrial regions in Northeast China,
454 Meteorol. Atmos. Phys., 127, 345-354, 10.1007/s00703-015-0367-3, 2015.
- 455 Che, H., Xia, X., Zhao, H., Dubovik, O., Holben, B. N., Goloub, P., Cuevas-Agulló, E.,
456 Estelles, V., Wang, Y., Zhu, J., Qi, B., Gong, W., Yang, H., Zhang, R., Yang, L.,
457 Chen, J., Wang, H., Zheng, Y., Gui, K., Zhang, X., and Zhang, X.: Spatial
458 distribution of aerosol microphysical and optical properties and direct radiative
459 effect from the China Aerosol Remote Sensing Network, Atmos. Chem. Phys.
460 Discuss., <https://doi.org/10.5194/acp-2019-405>, 2019.
- 461 Crawford, T. M., and Duchon, C. E.: An improved parameterization for estimating
462 effective atmospheric emissivity for use in calculating daytime downwelling
463 longwave radiation, J. Appl. Meteorol., 38, 474–480, 1998.
- 464 Deardorff, J. W.: Efficient prediction of ground surface temperature and moisture, with
465 an inclusion of a layer of vegetation. J. Geophys. Res., 83, 1889–1903, 1978.
- 466 Dilley, A. C., and O'Brien, D. M.: Estimating downward clear sky long-wave irradiance
467 at the surface from screen temperature and precipitable water, Q. J. Roy. Meteorol.
468 Soc., 124a, 1391–1401, 1997.
- 469 Dozier, J., and Frew, J.: Rapid calculation of terrain parameters for radiation modeling
470 from digital elevation data, IEEE T. Geosci. Remote, 28, 963–969, 1990.

471 Dominik, M., R. Philipona, C. Ruckstuhl, R. Vogt and L. Vuilleumier, Performance and
472 uncertainty of CNR1 net radiometers during a one-year field comparison, *J of*
473 *Atmos., and Ocean. Tech.*, 25(3), 442-451, 2008.

474 Duan, A., and Wu, G.: Change of cloud amount and the climate warming on the Tibetan
475 Plateau, *Geophys. Res. Lett.*, 33, 10.1029/2006gl027946, 2006.

476 Duarte, H. F., Dias, N. L., and Maggioletto, S. R.: Assessing daytime downward
477 longwave radiation estimates for clear and cloudy skies in Southern Brazil, *Agr.*
478 *Forest. Meteorol.*, 139, 171-181, 10.1016/j.agrformet.2006.06.008, 2006.

479 Duchon, C. E., and O'Malley, M. S.: Estimating cloud type from pyranometer
480 observations, *J. Appl. Meteorol.*, 38, 132-141, 1999.

481 Dupont, J. C., Haeffelin, M., Drobinski, P., and Besnard, T.: Parametric model to
482 estimate clear-sky longwave irradiance at the surface on the basis of vertical
483 distribution of humidity and temperature, *J. Geophys. Res.*, 113,
484 10.1029/2007jd009046, 2008.

485 Durr, B., and Philipona, R.: Automatic cloud amount detection by surface longwave
486 downward radiation measurements, *J. Geophys. Res.*, 109, 9,
487 10.1029/2003jd004182, 2004.

488 Gubler, S., Gruber, S., and Purves, R. S.: Uncertainties of parameterized surface
489 downward clear-sky shortwave and all-sky longwave radiation, *Atmos. Chem.*
490 *Phys.*, 12, 5077-5098, 10.5194/acp-12-5077-2012, 2012.

491 He, Q. S., Li, C. C., Ma, J. Z., Wang, H. Q., Shi, G. M., Liang, Z. R., Luan, Q., Geng,
492 F. H., and Zhou, X. W.: The properties and formation of cirrus clouds over the
493 Tibetan Plateau based on summertime lidar measurements, *J. Atmos. Sci.*, 70, 901-
494 915, 10.1175/jas-d-12-0171.1, 2013.

495 Idso, S. B.: A set of equations for full spectrum and 8 to 14 μm and 10.5 to 12.5 μm
496 thermal radiation from cloudless skies, *Water Resource Res.*, 17, 295–304, 1981.

497 Iqbal, M.: *An Introduction to Solar Radiation*, Academic Press, Toronto, Canada, 1983.

498 Iziomon, M. G., Mayer, H., and Matzarakis, A.: Downward atmospheric longwave
499 irradiance under clear and cloudy skies: measurement and parameterization, *J.*
500 *Atmos. Solar-Terr. Phys.*, 65, 1107–1116, 2003.

501 Jacobs, J.D.: Radiation climate of Broughton Island, in: *Energy Budget Studies in*
502 *Relation to Fast-ice Breakup Processes in Davis Strait*, edited by Barry, R. G. and
503 Jacobs, J. D., *Inst. of Arctic and Alp. Res. Occas. Paper No. 26*. University of
504 Colorado, Boulder, pp. 105–120, 1978.

505 James, G., Witten, D., Hastie, T., and Tibshirani, R.: An Introduction to Statistical
506 Learning: with Applications in R, Springer-Verlag New York, USA, 2013.

507 Kato, S., Rose, F., Sun, S., Miller, W., Chen, Y., Rutan, D., Stephens, G., Loeb, N.,
508 Minnis, P., Wielicki, B., Winker, D., Charlock, T., Stackhouse Jr, P., Xu, K. M.,
509 and Collins, W.: Improvements of top-of-atmosphere and surface irradiance
510 computations with CALIPSO-, CloudSat-, and MODIS-derived cloud and aerosol
511 properties, *J. Geophys. Res.*, 116, D19209, 10.1029/2011JD016050, 2011.

512 Kiehl, J. T., and Trenberth, K. E.: Earth's annual global mean energy budget. *Bull. Am.*
513 *Meteorol. Soc.*, 78, 197-208, 1997.

514 Konzelmann, T., van de Wal, R. S. W., Greuell, W., Bintanja, R., Henneken, E. A. C.,
515 and Abe-Ouchi, A.: Parameterization of global and longwave incoming radiation
516 for the Greenland Ice Sheet, *Global Planet. Change*, 9, 143–164, 1994.

517 Kruk, N. S., Vendrame, I. F., da Rocha, H. R., Chou, S. C., and Cabral, O.: Downward
518 longwave radiation estimates for clear and all-sky conditions in the Sertozinho
519 region of So Paulo, Brazil, *Theor. Appl. Climatol.*, 99, 115-123, 2010.

520 Li, M. Y., Jiang, Y. J., and Coimbra, C. F. M.: On the determination of atmospheric
521 longwave irradiance under all-sky conditions, *Sol. Energy.*, 144, 40-48,
522 10.1016/j.solener.2017.01.006, 2017.

523 Liang, H., Zhang, R. H., Liu, J. M., Sun, Z. A., and Cheng, X. H.: Estimation of hourly
524 solar radiation at the surface under cloudless conditions on the Tibetan Plateau
525 using a simple radiation model, *Adv. Atmos. Sci.*, 29, 675-689, 10.1007/s00376-
526 012-1157-1, 2012.

527 Long, C. N., Ackerman, T. P., Gaustad, K. L., and Cole, J. N. S.: Estimation of fractional
528 sky cover from broadband shortwave radiometer measurements, *J. Geophys. Res.*,
529 111, 11, 10.1029/2005jd006475, 2006.

530 Long, C. N., and Turner, D. D.: A method for continuous estimation of clear-sky
531 downwelling longwave radiative flux developed using ARM surface
532 measurements, *J. Geophys. Res.*, 113, 16, 10.1029/2008jd009936, 2008.

533 Marthews, T. R., Malhi, Y., and Iwata, H.: Calculating downward longwave radiation
534 under clear and cloudy conditions over a tropical lowland forest site: an evaluation
535 of model schemes for hourly data, *Theor. Appl. Climatol.*, 107, 461-477,
536 10.1007/s00704-011-0486-9, 2012.

537 Marty, C., and Philipona, R.: The Clear-Sky Index to separate clear-sky from cloudy-
538 sky situations in climate research, *Geophys. Res. Lett.*, 27, 2649-2652,

539 10.1029/2000gl011743, 2000.

540 Maykut, G. A., and Church P. E.: Radiation climate of Barrow, Alaska, 1962–1966, *J.*
541 *Appl. Meteorol.*, 12, 620–628, 1973.

542 Niemelä, S., Räisänen, P., and Savijärvi, H.: Comparison of surface radiative flux
543 parameterizations: Part I: Longwave radiation, *Atmos. Res.*, 58, 1–18, 2001a.

544 Orsini, A., Tomasi, C., Calzolari, F., Nardino, M., Cacciari, A., and Georgiadis, T.:
545 Cloud cover classification through simultaneous ground-based measurements of
546 solar and infrared radiation, *Atmos. Res.*, 61, 251-275, 10.1016/s0169-
547 8095(02)00003-0, 2002.

548 Prata, A. J.: A new long-wave formula for estimating downward clear-sky radiation at
549 the surface, *Q. J. Roy. Meteorol. Soc.*, 122, 1127–1151, 1996.

550 Rangwala, I., Miller, J. R., and Xu, M.: Warming in the Tibetan plateau: possible
551 influences of the changes in surface water vapor. *Geophys. Res. Lett.*, 36, 295-311,
552 2009.

553 Satterlund, D. R.: An improved equation for estimating longwave radiation from the
554 atmosphere, *Water Resource Res.*, 15, 1649–1650, 1979.

555 Stephens, G. L., Wild, M., Stackhouse, P. W., Jr., L'Ecuyer, T., Kato, S., and Henderson,
556 D. S.: The global character of the flux of downward longwave radiation, *J.*
557 *Climate.*, 25, 2329-2340, 10.1175/jcli-d-11-00262.1, 2012.

558 Stoffel, T.: Solar infrared radiation station (SIRS) handbook, Tech. Rep., ARM TR-025,
559 *Atmos. Rad. Mea. Program*, U.S. Dep. of Energy, Washington, D.C, 2005.

560 Sugita, M., and Brutsaert, W.: Cloud effect in the estimation of instantaneous downward
561 longwave radiation, *Water Resource Res.*, 29, 599-605, 10.1029/92wr02352, 1993.

562 Swinbank, W. C.: Long-wave radiation from clear skies, *Q. J. Roy. Meteo. Soc.*, 89,
563 330–348, 1963.

564 Viúdez-Mora, A., Costa-Surós, M., Calbó, J., and González, J. A.: Modeling
565 atmospheric longwave radiation at the surface during overcast skies: The role of
566 cloud base height, *J. Geophys. Res. Atmos.*, 120, 199–214, 10.1002/
567 2014JD022310, 2015.

568 Wang, K., and Liang, S.: Global atmospheric downward longwave radiation over land
569 surface under all-sky conditions from 1973 to 2008, *J. Geophys. Res.*, 114,
570 10.1029/2009jd011800, 2009.

571 Wang, K., and Dickinson, R. E.: Global atmospheric downward longwave radiation at
572 the surface from ground-based observations, satellite retrievals, and re-analyses,

573 Reviews of Geophysics, 51, 150-185, 10.1002/rog.20009, 2013.

574 Yang, K., Ding, B., Qin, J., Tang, W., Lu, N., and Lin, C.: Can aerosol loading explain
575 the solar dimming over the Tibetan Plateau? *Geophys. Res. Lett.*, 39,
576 10.1029/2012gl053733, 2012.

577 Zhao X., Peng B., Qin N., Wang W. (2011), Characteristics of Energy Transfer and
578 Micrometeorology in Surface Layer in Different Areas of Tibetan Plateau in
579 Summer (in Chinese), *Plateau and mountain Meteorology Research*,31(1), 6-11,
580 2011.

581 Zhu, M. L., Yao, T. D., Yang, W., Xu, B. Q., and Wang, X. J.: Evaluation of
582 parameterizations of incoming longwave radiation in the high-mountain region of
583 the Tibetan Plateau, *J. Appl. Meteorol. Climatol.*, 56, 833-848, 10.1175/jamc-d-
584 16-0189.1, 2017.

585

586

587 Table 1: Description of stations and measurements (magnitude and variability) in the

588

Tibetan Plateau

Site	Altitude (m ASL)	Period	T (°C)	e (hPa)	DLR ($\text{W}\cdot\text{m}^{-2}$)	Data Points
NQ	4507	2011.7.20- 2011.8.26	9.4 ± 8	7.4 ± 5	242.75 ± 40	52980
NC	2290	2014.6.7- 2014.7.31	16.8 ± 10	13.4 ± 4	368.25 ± 40	69609
AL	4279	2016.5.27- 2016.9.22	7.8 ± 4	4.8 ± 4	253.11 ± 50	86596

589

590

Table 2. 11 clear-sky DLR parameterizations and their specific conditions

Reference	Clear-Sky Parameterization	Conditions
Angstrom (1915)	$DLR_{clr} = \{0.83 - 0.18 \times 10^{-0.067e}\} \sigma T^4$	Alt.: 1650~3500 T: 283.15~303.15 e: 4~1
Brunt (1932)	$DLR_{clr} = (0.52 + 0.065\sqrt{e}) \sigma T^4$	Alt.: 6~3500 T: 269.15~303.15 e: 2.5~16
Swinbank (1963)	$DLR_{clr} = 5.31 \times 10^{-13} T^6$	Alt.: 2 T: 281.15~302.15 e: 8~30
Idso and Jackson (1969)	$DLR_{clr} = (1 - 0.261 \cdot \exp(-0.000777 \times (273 - T)^2)) \sigma T^4$	Alt.: 3, 331 T: 228.15~318.15
Brutsaert (1975)	$DLR_{clr} = 1.24 \left(\frac{e}{T}\right)^{\frac{1}{7}} \sigma T^4$	Alt.: 6~3500 T: 269.15~313.15 e: 2.5~16
Satterlund (1979)	$DLR_{clr} = 1.08 \left(1 - \exp\left(-e^{\frac{T}{2016}}\right)\right) \sigma T^4$	Alt.: 594 T: 236.15~309.15 e: 0~18hPa
Idso (1981)	$DLR_{clr} = \left(0.7 + 5.95 \times 10^{-5} \times e \times \exp\left(\frac{1500}{T}\right)\right) \sigma T^4$	Alt.: 331 T: 258.15~278.15 e: 2~6
Konzelmann (1994)	$DLR_{clr} = \left(0.23 + 0.443 \left(\frac{e}{T}\right)^{\frac{1}{8}}\right) \sigma T^4$	Alt.: 340~3230 T: 257.15~279.15 e: 1.5~5.5
Prata (1996)	$DLR_{clr} = (1 - (1 + 46.5 \frac{e}{T}) \times \exp(-(1.2 + 3 \times 46.5 \frac{e}{T})^{0.5})) \sigma T^4$	Not specified
Dilley and O'Brien (1998)	$DLR_{clr} = 59.38 + 113.7 \left(\frac{T}{273.16}\right)^6 + 96.96 \sqrt{46.5 \frac{e}{T} / 2.5}$	Not specified
Iziomon (2001)	$DLR_{clr} = \left(1 - 0.43 \exp\left(-\frac{11.5e}{T}\right)\right) \sigma T^4$	Alt.: 1489 $\bar{T} = 277.55 \bar{e} = 7.4$

592 *Where Alt. is the altitude above sea level, and its unit is (m ASL), e is screen-level water vapor
593 pressure in hPa and T represents surface temperature in K

594

595

Table 3. Locally fitted clear-sky DLR parameterizations in TP

Reference	Locally fitted Clear-Sky Parameterization
Angstrom(1915)	$DLR_{clr} = \{0.8 - 0.19 \times 10^{-0.068e}\} \sigma T^4$
Brunt(1932)	$DLR_{clr} = (0.56 + 0.07\sqrt{e}) \sigma T^4$
Swinbank(1963)	$DLR_{clr} = 4.7 \times 10^{-13} T^6$
Idso & Jackson(1969)	$DLR_{clr} = (1 - 0.36 \cdot \exp(-0.00065 \times (273 - T)^2)) \sigma T^4$
Brutsaert(1975)	$DLR_{clr} = 1.03 \left(\frac{e}{T}\right)^{0.09} \sigma T^4$
Satterlun (1979)	$DLR_{clr} = \left(1 - \exp\left(-e^{\frac{T}{2016}}\right)\right) \sigma T^4$
Idso(1981)	$DLR_{clr} = \left(0.63 + 7.5 \times 10^{-5} \times e \times \exp\left(\frac{1500}{T}\right)\right) \sigma T^4$
Konzelmann(1994)	$DLR_{clr} = \left(0.23 + 0.45 \left(\frac{e}{T}\right)^{0.13}\right) \sigma T^4$
Prata(1996)	$DLR_{clr} = (1 - (1 + 46.5 \frac{e}{T}) \times \exp(-(1 + 3 \times 46.5 \frac{e}{T})^{0.5})) \sigma T^4$
Dilley and O'Brien(1998)	$DLR_{clr} = -2.54 + 158.1 \left(\frac{T}{273.16}\right)^6 + 106.4 \sqrt{46.5 \frac{e}{T} / 2.5}$
Iziomon(2001)	$DLR_{clr} = \left(1 - 0.38 \exp\left(-\frac{14.52e}{T}\right)\right) \sigma T^4$

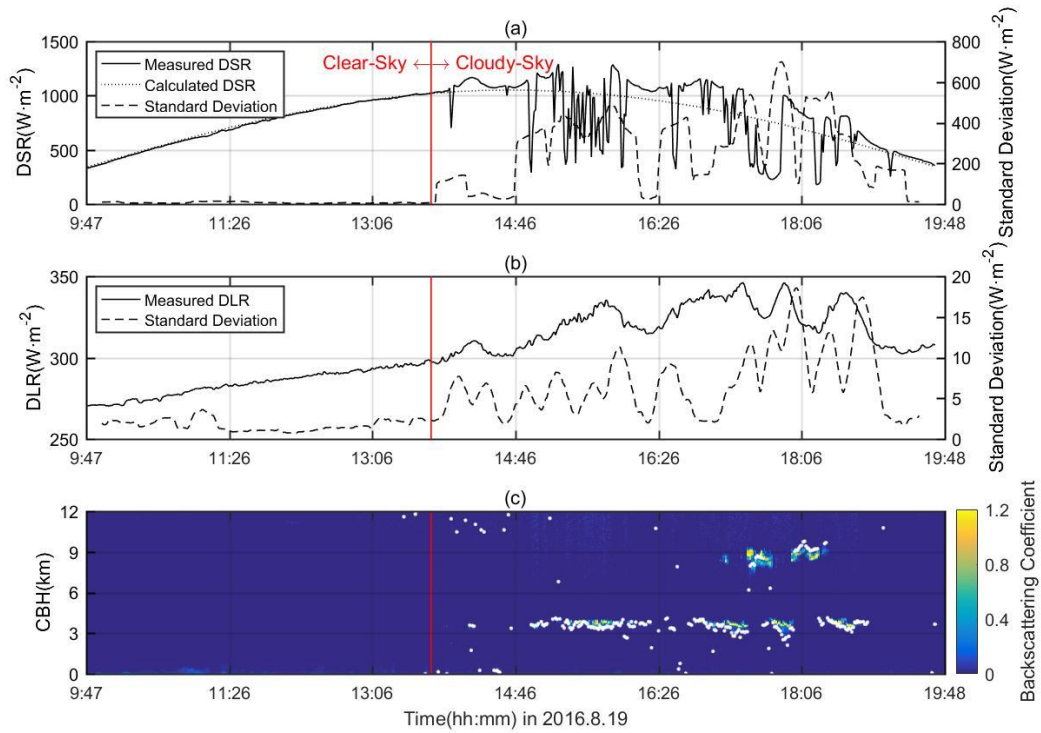
Table 4. 4 Ordinary and locally fitted cloudy-sky DLR parameterizations

Reference	DLR _{cl} Parameterization	Ordinary Parameters	Locally Fitted Parameters
Maykut(1973)	$(a + b \times CF^c)\sigma T^4$	a=0.7855 b=0.000312 c=2.75	a=0.85 b=0.01 c=3
Jacobs(1978)	$(1 + a \times CF)DLR_{clr}$	a=0.26	a=0.23
Sugita(1993)	$(1 + a \times CF^b) DLR_{clr}$	a=0.0496 b=2.45	a=0.2 b=1.3
Konzelmann(1994)	$(1 - CF^a)DLR_{clr} + b \times CF^a\sigma T^4$	a=4 b=0.95	a=3.5 b=1

600

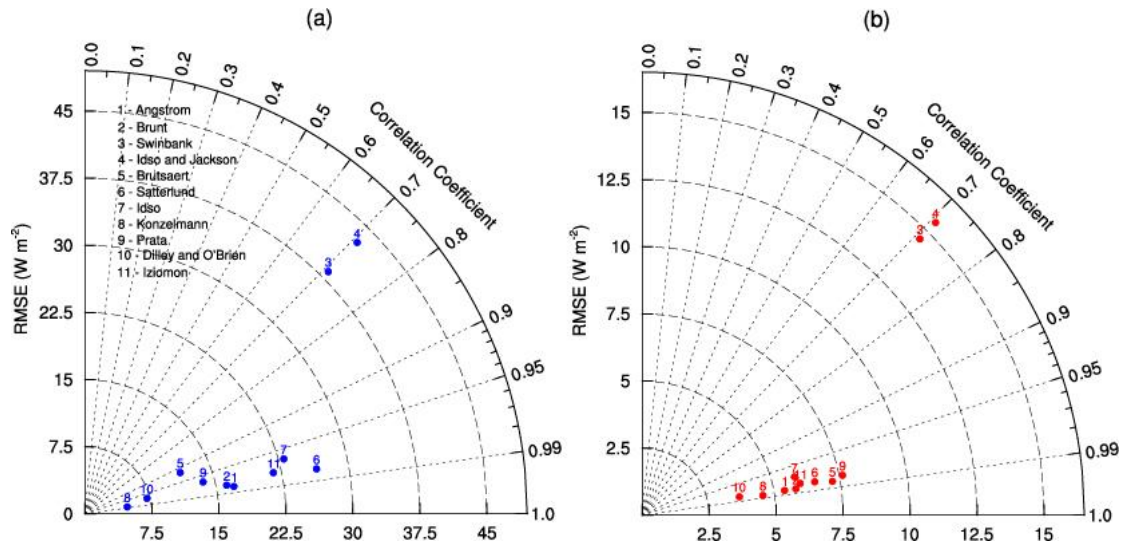
601

602



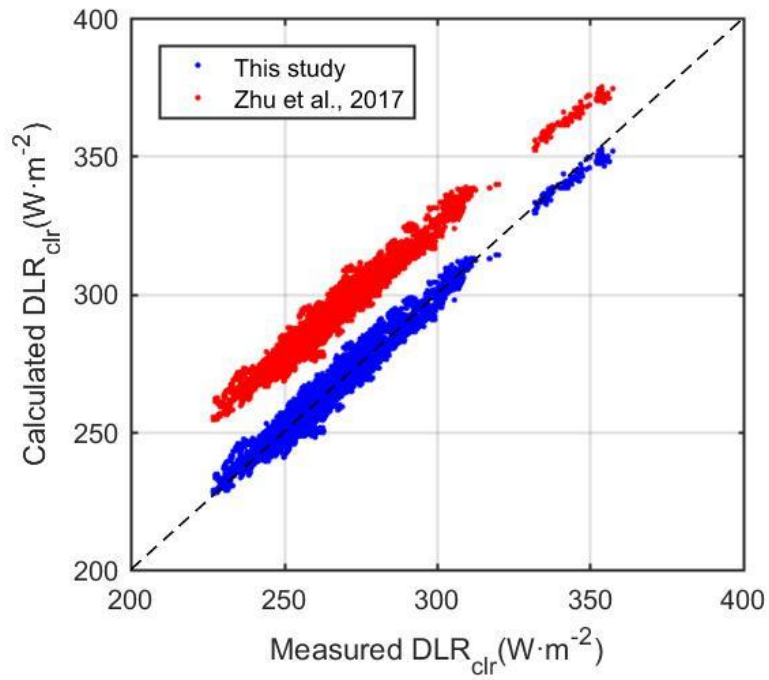
603

604 Fig. 1. Time series of data sample on 2016.8.19 transited from clear-sky to cloudy-sky: (a)
 605 measured (black line) and calculated (dotted black line) downward shortwave radiation and its 21-
 606 min standard deviation (grey line), (b) measured downward longwave radiation and 21-min standard
 607 deviation and (c) MPL backscattering coefficient and the cloud base height.



608
 609
 610
 611

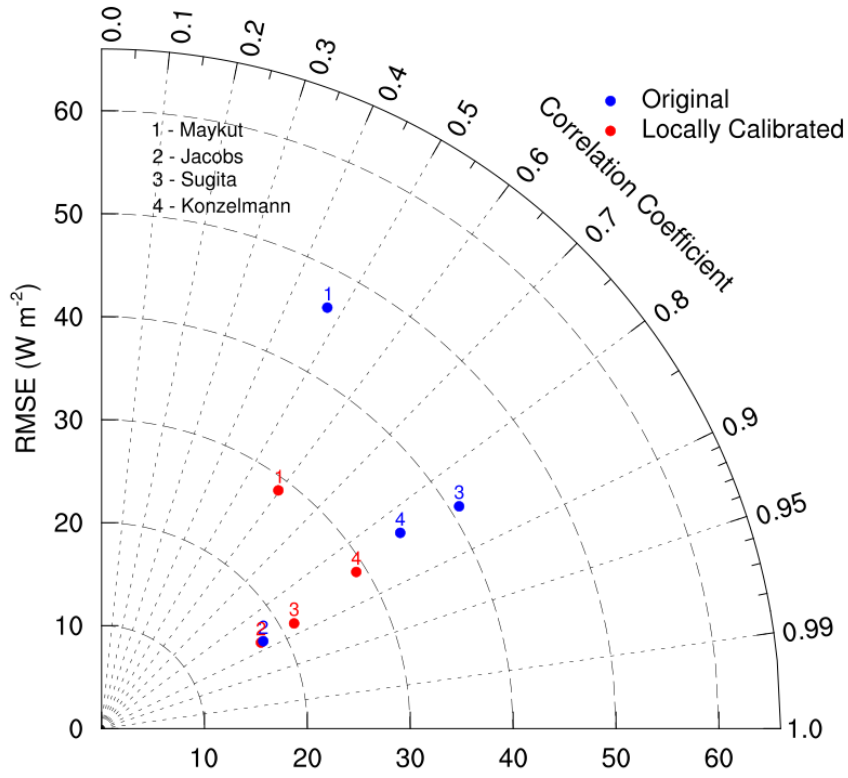
Fig. 2. RMSE and R^2 for the clear-sky DLR parameterizations using original (a) and locally calibrated (b) coefficients.



613

614 Fig. 3. Scatter plots of measured clear-sky DLR data from as a function of calculations
615 by the Eq.(3) this study (blue dots) and the Eq.(4) by Zhu et al. (2017) (red dots). The
616 dash black line is the 1:1 line.

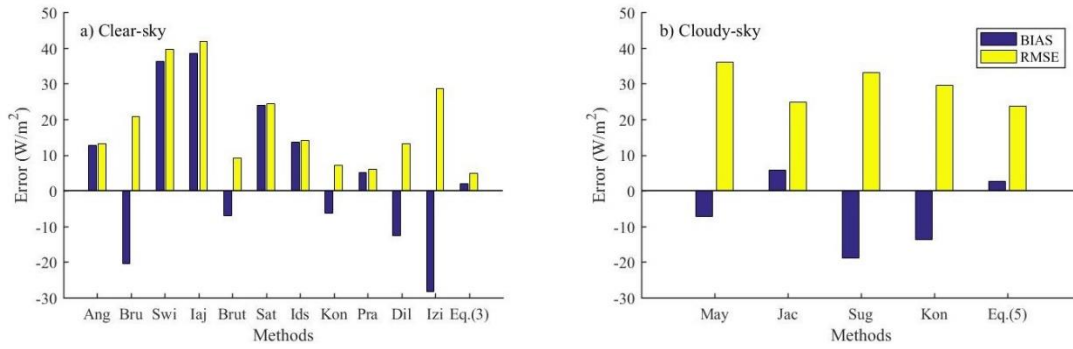
617



618

619 Fig. 4. RMSE and R^2 for the cloudy-sky DLR (DLR_{cld}) parameterizations using the
 620 original (blue) and locally calibrated (red) coefficient.

621

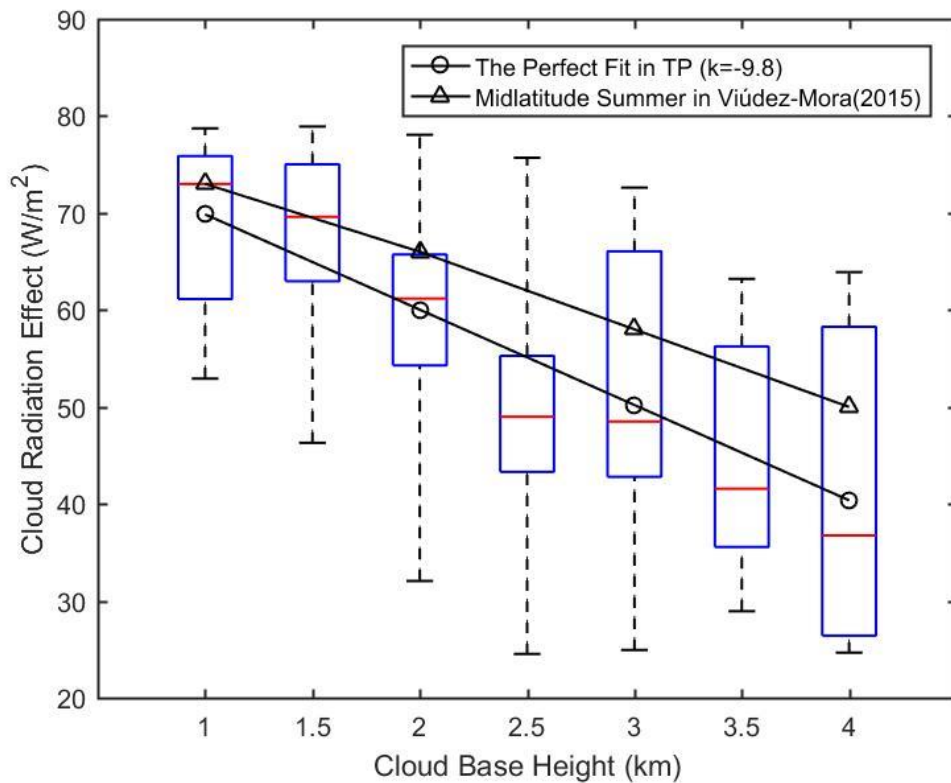


622

623 Fig. 5. The bias and RMSE for the LDR parameterizations using (a) the published
 624 clear-sky and Eq.(3), and (b) cloudy-sky parameterizations and Eq.(5).

625

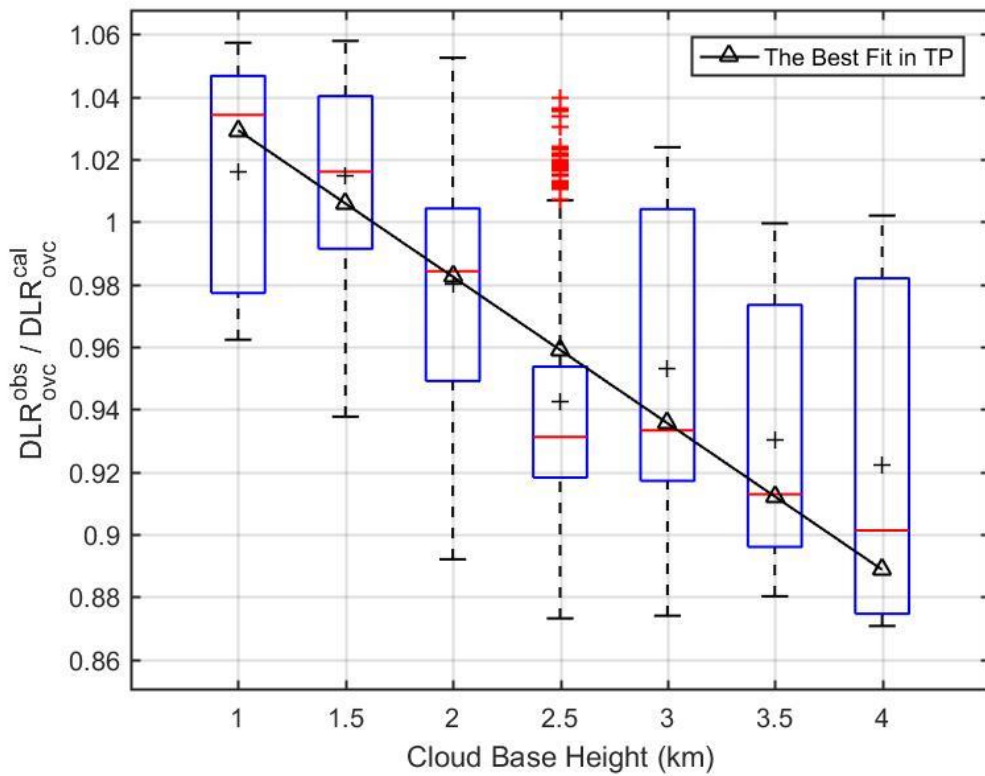
626



628

629 Fig. 6. Distributions of cloud radiative effect against measured cloud base height are
 630 represented by box plot (the blue box indicates the 25th and 75th percentiles, the
 631 whiskers indicate 5th and 95th percentiles, the red middle line is the median). The black
 632 circles line and the black triangles is mean values of cloud radiative effect over TP in
 633 this study and in midlatitude site (Girona, Spain) in Viúdez-Mora(2015) respectively.

634



635

636 Fig. 7. Distributions of the ratio of observed DLR and calculated DLR by Eq.(5) under
 637 overcast condition against measured cloud base height are represented by box plot (the
 638 blue box indicates the 25th and 75th percentiles, the whiskers indicate 5th and 95th
 639 percentiles, the red middle line is the median, the black plus sign is the mean). The
 640 black triangle line is the fitting line.

641

642

643